Wolfgang E. Nagel
Dietmar H. Kröner
Michael M. Resch *Editors*

High Performance Computing in Science and Engineering '21

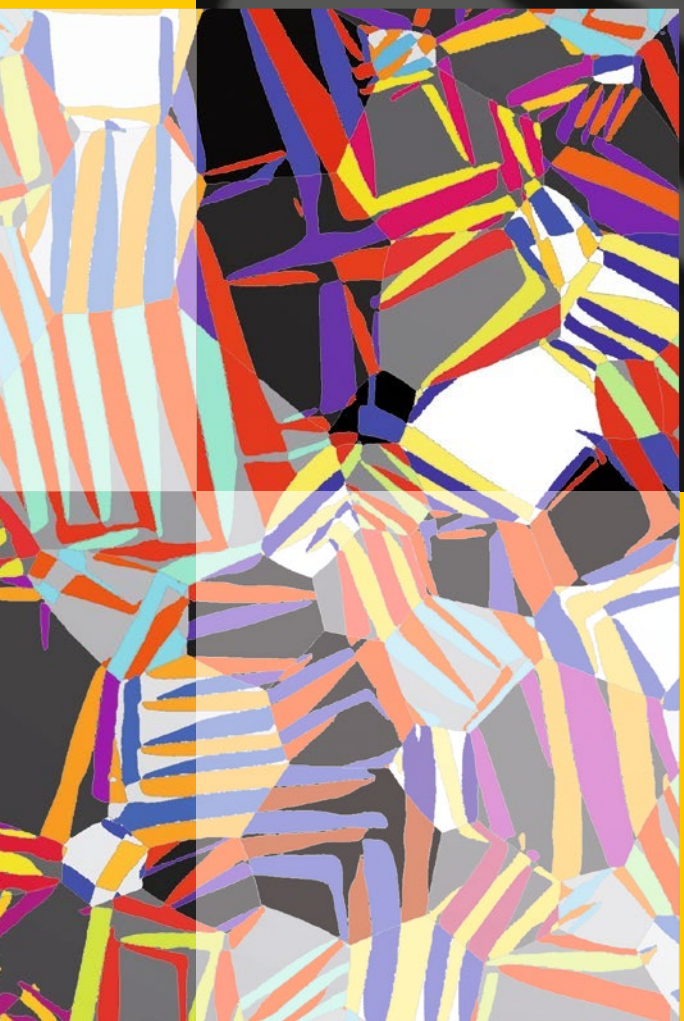

H L R S

Springer

High Performance Computing in Science and Engineering ’21

Wolfgang E. Nagel • Dietmar H. Kröner
Michael M. Resch
Editors

High Performance Computing in Science and Engineering ’21

Transactions of the High Performance Computing Center, Stuttgart (HLRS) 2021

Springer

Editors
Wolfgang E. Nagel
Zentrum für Informationsdienste
und Hochleistungsrechnen (ZIH)
Technische Universität Dresden
Dresden, Germany

Dietmar H. Kröner
Abteilung für Angewandte
Mathematik
Universität Freiburg
Freiburg, Germany

Michael M. Resch
Höchstleistungsrechenzentrum
Stuttgart (HLRS)
Universität Stuttgart
Stuttgart, Germany

ISBN 978-3-031-17936-5 ISBN 978-3-031-17937-2 (eBook)
https://doi.org/10.1007/978-3-031-17937-2

Mathematics Subject Classification (2020): 65Cxx, 65C99, 68U20, 90-08, 97M50

Cover illustration: The image shows the resulting polycrystalline microstructure of a martensitic phase transformation predicted by a multiphase-field simulation performed with PACE3D. The regions shown in shades of gray represent retained austenite, while the regions depicted in color are martensitic variants. Details can be found in “High-performance multiphase-field simulations of solid-state phase transformations using PACE3D” by E. Schoof, T. Mittnacht, M. Seiz, P. Hoffrogge, H. Hierl, and B. Nestler, Institute of Applied Materials (IAM), Karlsruhe Institute of Technology (KIT), Straße am Forum 7, 76131 Karlsruhe, Germany, on pages 167ff.

This Springer imprint is published by the registered company Springer Nature Switzerland AG
The registered company address is: Gewerbestrasse 11, 6330 Cham, Switzerland

Contents

Physics

In this part, three physics projects are presented, which achieved important scientific results in 2020/21 by using Hawk/Hazel Hen at the HLRS and ForHLR II of the Steinbuch Center.

Fascinating new results are being presented in the following pages on soft matter/biochemical systems (ligand-induced protein stabilization) and on quantum systems (anomalous magnetic moment of the muon, ultracold-boson quantum simulators, phase transitions, resonant tunneling, and variances).

Studies of the soft matter/biochemical systems have focused on ligand-induced protein stabilization.

T. Schäfer, A.C. Joerger, J. Spencer, F. Schmid, and G. Settanni from Mainz (T.S., F.S., G.S.), Frankfurt (A.C.J.), and Sussex (J.S.) present interesting new results on ligand-induced protein stabilization in their project *Flexadfg*. The authors show how Molecular Dynamics simulations of several cancer mutants of the DNA-binding domain of the tumor suppressor protein p53 allowed to establish the destabilizing effect of the mutations as well as the stabilizing effects of bound ligands. In addition, the authors report on the development of a new reweighting technique for metadynamics simulations that speeds up convergence and may provide an advantage in the case of simulations of large systems.

Studies of the quantum systems have focused on the anomalous magnetic moment of the muon, and on ultracold-boson quantum simulators, phase transitions, resonant tunneling, and variances.

M. Cè, E. Chao, A. Gérardin, J.R. Green, G. von Hippel, B. Hörz, R.J. Hudspith, H.B. Meyer, K. Miura, D. Mohler, K. Ottnad, S. Paul, A. Risch, T. San José, and H. Wittig from Mainz (E.C., G.v.H., R.J.H., H.B.M., K.M., K.O., S.P., T.S.J., H.W.), Darmstadt (K.M., D.M., T.S.J.), Zeuthen (A.R.), Geneva (M.C., J.R.G.), Marseille (A.G.), and Berkeley (B.H.) present interesting results obtained by their lattice QCD Monte Carlo simulations on Hawk/Hazel Hen in their project *GCS-HQCD* on leading hadronic contributions to the anomalous magnetic moment of the muon, on the energy dependence of the electromagnetic coupling, on the electroweak mixing angle, and on the hadronic vacuum polarisation and light-by-light scattering contributions.

The authors focus will turn to increasing the overall precision of their determination of the hadronic vacuum polarization contribution to the muon anomalous magnetic moment to the sub-percent level.

A.U.J. Lode, O.E. Alon, J. Arnold, A. Bhowmik, M. Büttner, L.S. Cederbaum, B. Chatterjee, R. Chitra, S. Dutta, C. Georges, A. Hemmerich, H. Keßler, J. Klinder, C. Lévêque, R. Lin, P. Molignini, F. Schäfer, J. Schmiedmayer, and M. Žonda from Freiburg (A.U.J.L., M.B.), Haifa (O.E.A., A.B., S.D.), Basel (J.A., F.S.), Heidelberg (L.S.C.), Kanpur (B.C.), Zürich (R.C., R.L.), Hamburg (C.G., A.H., H.K., J.K.), Wien (C.L., J.S.), Oxford (P.M.), and Prague (M.Z.) present interesting results obtained in their project *MCTDHB* with their multiconfigurational time-dependent Hartree method for indistinguishable particles (MCTDH-X) on Hazel Hen and Hawk. In the past the authors have implemented their method to solve the many-particle Schrödinger equation for time-dependent and time-independent systems in various software packages. The authors present interesting new results of their investigations on ultracold boson quantum simulators for crystallization and superconductors in a magnetic field, on phase transitions of ultracold bosons interacting with a cavity, and of charged fermions in lattices described by the Falicov–Kimball model. In addition, the authors report on new results on the many-body dynamics of tunneling and variances, in two- and three-dimensional ultracold-boson systems.

Fachbereich Physik,
Universität Konstanz,
78457 Konstanz,
Germany,
e-mail: peter.nielaba@uni-konstanz.de

Peter Nielaba

Ligand-induced protein stabilization and enhanced molecular dynamics sampling techniques

Timo Schäfer, Andreas C. Joerger, John Spencer, Friederike Schmid and Giovanni Settanni

Abstract Molecular dynamics (MD) simulations provide an increasingly important instrument to study protein-materials interaction phenomena, thanks to both the constant improvement of the available computational resources and the refinement of the modeling methods. Here, we summarize the results obtained along two different research directions within our project. First, we show how MD simulations of several cancer mutants of the DNA-binding domain of the tumor suppressor protein p53 allowed to establish the destabilizing effect of the mutations as well as the stabilizing effects of bound ligands. Second, we report on the development of a new reweighting technique for metadynamics simulations that speeds up convergence and may provide an advantage in the case of simulation of large systems.

1 Introduction

Molecular dynamics (MD) simulations provide a way to observe the motions of molecular objects at the atomic scale. In classical MD simulations, each system is composed of a set of particles and is represented by a Hamiltonian energy function of the coordinates and momenta of the particles. By numerical integration of the Hamiltonian equations of motion, MD allows to follow the trajectories of all the particles as a function of time and, in this way, to extrapolate its static and dynamic properties. A crucial step to guarantee the accuracy of the observations is the

Timo Schäfer, Friederike Schmid and Giovanni Settanni
Department of Physics, Johannes Gutenberg University, Mainz, Germany,
e-mail: settanni@uni-mainz.de

Andreas C. Joerger
Institute of Pharmaceutical Chemistry, Johann Wolfgang Goethe University, Frankfurt am Main, Germany

John Spencer
Department of Chemistry, School of Life Sciences, University of Sussex, United Kingdom

W. E. Nagel et al. (eds.), *High Performance Computing in Science and Engineering '21*,
https://doi.org/10.1007/978-3-031-17937-2_1

availability of highly optimized force fields, i.e., the classical Hamiltonian function, which approximates the underlying quantum chemical nature of the system. During the course of the last 40 years, MD force fields for the simulations of biomolecules have been dramatically improved in terms of accuracy to the point that it is now possible to simulate phenomena like protein folding, at least for some small proteins [1], as well as protein-ligand and protein-materials interactions [2–11]. In this report, we will show how we have been able to use classical MD simulations to characterize the stability of several cancer mutants of p53, a protein that is found mutated in about 50% of the cancer cases diagnosed every year [12]. In that study simulations were used also to asses the effect of small ligands which, by binding to a mutation-induced pocket on the protein surface, are capable of stabilizing the protein, thus representing possible lead compounds for the development of cancer therapeutics. In addition to protein folding, many biological phenomena, however, occur on time scales that are still inaccessible to standard classical MD. For this reason, a wide range of enhanced sampling techniques have been proposed. Metadynamics [13–15] is one of the most popular techniques. In metadynamics, a time-dependent energy term is added to the Hamiltonian, to drive the system away from regions of conformational space already sampled. We started to use this method in the past to characterize the conformational properties of a large protein complex, fibrinogen [9]. We soon discovered that in this case, the available methods to unbias the metadynamics sampling and obtain an equilibrium distribution of the most significant observables of the system were inadequate. We have then developed a new method, which is more accurate than those previously available in the limit of short trajectories [16]. In what follows, we also review these findings.

2 Methods

GROMACS[17] was used to perform the MD simulations. GROMACS exploits intra-node OpenMP parallelization and inter-node MPI parallelization and was optimally compiled to run efficiently both on Hazelhen and on Hawk HPC infrastructures at HLRS. Unless stated differently, in what follows, the simulations were performed with the CHARMM36m force field [18], while the ligands were modeled using the Charmm Generalized force field (CGenFF)[19]. The time step for the simulations was set to 2 fs. The LINCS [20] algorithm was used to constrain the length of bonds involving hydrogen atoms. A cut-off of 1.2 nm with a switch function starting at 1.0 nm was used for direct non-bonded interactions. A cell-list like algorithm [21] was used. Periodic boundary conditions were adopted along all directions and a smooth particle-mesh Ewald (sPME) approach [22] was used for long-range electrostatics. The water was modeled explicitly using a modified TIP3P model[23]. Pressure and temperature were regulated at 1 atm and 300 K, using the Parrinello–Rahman [24] and Nose–Hoover [25, 26] algorithms, respectively. Few water molecules were replaced by sodium and chlorine ions during simulation setup to neutralize the charge of the simulation box and to achieve the physiological ion concentration (0.15 M).

In the case of the p53 DNA-binding domain, the simulations were based on the structure of a stabilized pseudo-wild-type (pdb id 1UOL) [27] and mutant structures determined by X-ray crystallography or modeled in ref. [28]. The systems were minimized for a max 50'000 steps, then equilibrated in the NVT ensemble for 1 ns with positional restraints on the heavy atoms of the protein. Then, they were further equilibrated for 1 ns in the NPT ensemble with no restraints. Four production runs were started for each mutant. Each run was 200 ns long. Further methodological details are provided in the original publication ref. [28]. System sizes ranged from 37000 to 43000 atoms, which are sufficient to ensure good scaling on Hazelhen and Hawk running on 100 and 64 nodes, respectively. Simulations were set up as job chains with each job not exceeding 3 hours length, writing a single restart file at the end. The trajectories were analyzed using the program VMD [29] and WORDOM [30].

3 Simulations of p53 cancer mutants and stabilization by ligand binding

The tumor suppressor protein p53 is involved in several processes protecting the human genome, including activation of DNA repair mechanisms or induction of apoptosis (cell death) in case of extensive DNA damage. Mutations of this protein can often result in cancer and, indeed, mutations in this protein occur in half of the diagnosed cancers [12]. Among the most frequently found cancer mutations are those of residue 220 in the DNA-binding domain of the protein, with the most abundant being Y220C, found in about 100'000 new cancer cases each year. The wild-type protein (WT) (i.e., the one without mutations) is only marginally stable, and many cancer mutations induce a loss of stability, which reduces the folding transition temperature of the protein, leading to unfolding and, consequently, to a loss of function at body temperature. In some cases, such as Y220C, the mutation creates a crevice on the protein surface. This offers a possible strategy to reactivate the mutant protein: a drug that binds to the mutation-induced pocket may actually stabilize the protein and thereby rescue its tumor suppressor function. This strategy has already been successfully used to rescue the Y220C mutant [2, 31]. In collaboration with our experimental partners, we investigated other frequent cancer mutants with a mutation of Y220.

In ref. [28], we analyzed the cancer associated mutants Y220H, Y220N, Y220S, and Y220C using experimental biophysical techniques including, among others, X-ray crystallography as well as MD simulations. The latter have been used to estimate the effects of mutations on protein stability by monitoring the root-mean-square fluctuations (RMSF) [32], that is the average amplitude of the fluctuations of the atomic positions of the protein around the average structure. We used the same approach in the context of the p53 DNA-binding domain mutants, and we verified that the RMSF measured on the simulations correlated with experimentally determined differences in melting temperature of the mutant proteins (Tab. 1). Our simulations

also provided additional information complementing the structural data obtained by X-ray crystallography, for example, by sampling the dynamics of different regions of the protein. We monitored several atomic distances characterizing the mutation-induced crevice on the surface of the protein, which can be split into a central crevice and different subsites (Fig. 1). These distances did not show significant fluctuations in the WT, whereas in the cancer mutants, they fluctuated between two states which can be associated with open and collapsed conformations of the mutation-induced crevice (Fig. 1c).

Several carbazole-based compounds were shown to bind to the mutation-induced crevice in Y220C and stabilize the protein structure, thus increasing the folding transition temperature [2, 31]. Given the similarity between the crevices generated by the various mutations at site 220, in ref. [28] the effects of some of these carbazole compounds on the Y220S and Y220C mutants were analyzed. It was shown that several compounds that bind Y220C in the mutation-induced crevice can also bind to the equivalent pocket in Y220S, to a lesser extent also in the Y220N pocket. The binding of the compounds resulted in a considerable increase in the melting temperature of the mutants. MD simulations of the mutants in the presence of the carbazole compounds in the crevice revealed that the ligands dramatically reduced the RMSF of the protein, which correlated with the binding constant measured experimentally and the ligand-induced increase of the folding transition temperature (Tab. 1). In particular, the simulations showed that the collapsed state of the crevice is completely absent in the presence of the ligands (Fig. 2).

Summarizing this part of the report, the simulations of p53 DNA-binding domain mutants, with and without ligands, provided important insights into the molecular basis of the experimentally observed stabilizing effect upon binding. This information will aid the development of more potent small-molecule stabilizers and molecules targeting more than one mutant.

Codon 220 mutation	Average RMSF (Å)	Tm (°C)
Native structure		
WT	1.46	51.5
Y220H	1.56	45.1
Y220C	1.61	43.8
Y220N	1.64	39.9
Y220S	1.67	39.4
Ligand complexes		
Y220C-PK9323	1.35	
Y220S-PK9301	1.42	
Y220S-PK9323	1.58	

Table 1: Root-mean-square fluctuations (RMSF) of the simulated p53 DNA-binding domain constructs averaged over residues 97-289 and the experimentally determined folding transition temperature. Adapted from ref. [28], Bauer et al.

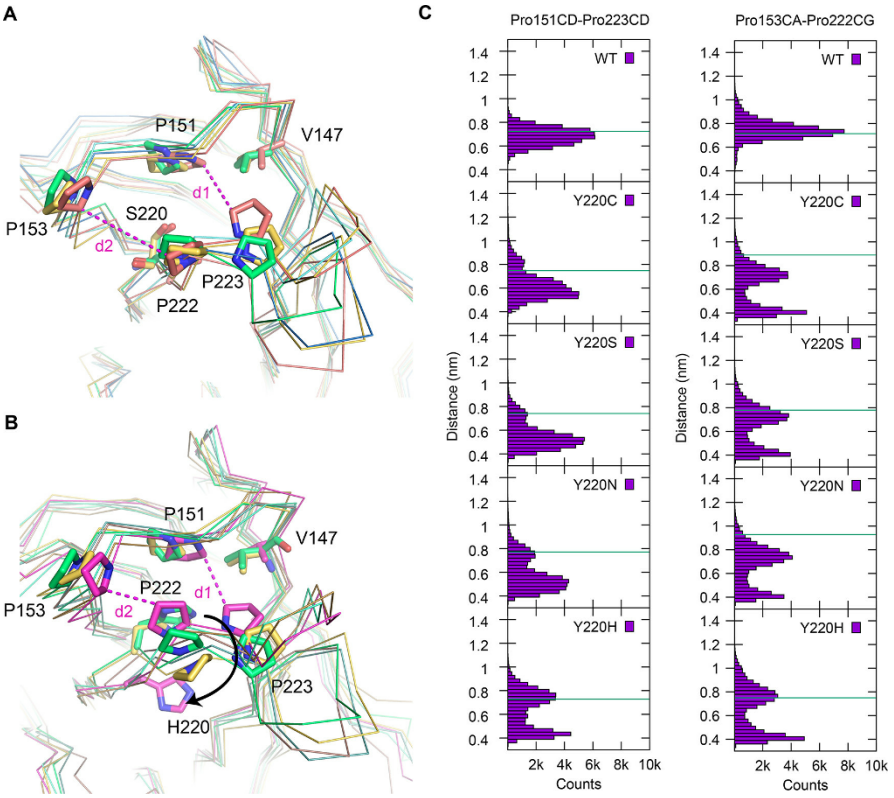

Fig. 1: MD simulation of p53 cancer mutants. (A) Representative C_α-trace structures of the open and closed states from the simulations of the p53 mutant Y220S superimposed onto the crystal structure (green). Highlighted residues are represented as sticks. Distances defining the size of the central cavity (d1) and the subsite 2 (d2) are represented with magenta dashed lines. (B) Same as (A) but for the Y220H mutant. The closed state is determined by the H220 side chain swinging out of the pocket. (C) Distribution of the d1 and d2 distances in the simulations of the p53 variants under consideration. The green line represent the distance in the crystal structure. Only WT shows an unimodal distribution. All mutants show the presence of a collapsed state of the crevice beside the open state. Adapted from ref. [28], Bauer et al. ©2020 licensed under CC-BY.

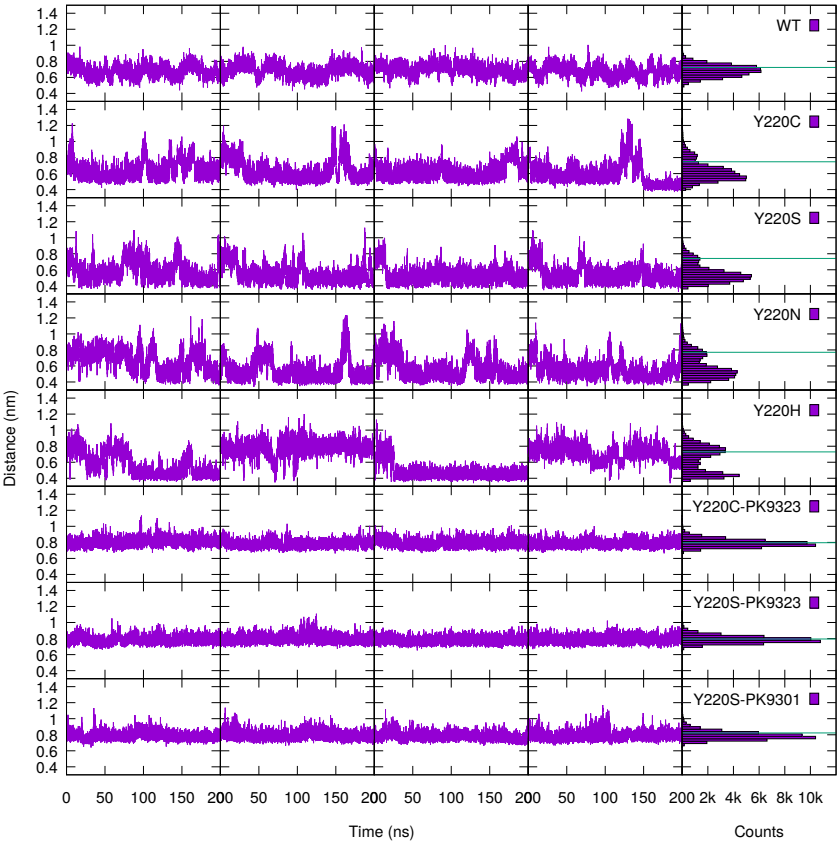

Fig. 2: Time series and resulting distributions of the d1 distance (see fig. 1) in all the simulated constructs. The presence of the ligands PK9323 and PK9301 in the crevice dramatically reduces structural fluctuations and prevents the population of collapsed states of the mutation-induced pocket. Adapted from ref. [28], Bauer et al. ©2020 licensed under CC-BY.

3.1 Data reweighting in metadynamics simulations

In this section, we review the results presented in ref. [16]. Metadynamics introduces a time-dependent bias potential in the classical energy of the system. The bias is dependent on selected collective variables $\boldsymbol{s}(\boldsymbol{r})$ of the system's coordinates, and it is built as a sum of Gaussian functions that are deposited at regular time intervals on the points reached by the trajectory:

$$V(\boldsymbol{s}(\boldsymbol{r}),t) = \sum_{t'=\Delta t,2\Delta t,\ldots}^{t} W\mathrm{e}^{-\sum_i^d (s_i(\boldsymbol{r})-s_i(\boldsymbol{r}(t')))^2/2\sigma_i^2} = \sum_{t'=\Delta t,2\Delta t,\ldots}^{t} g_{t'}(\boldsymbol{r},\boldsymbol{s}(t')) \quad (1)$$

where the Gaussian hills are $g_{t'}(\boldsymbol{s}(\boldsymbol{r})) = W\mathrm{e}^{-\sum_i^d (s_i(\boldsymbol{r})-s_i(\boldsymbol{r}(t')))^2/2\sigma_i^2}$. This results in pushing the system away from those values of the collective variables that have been already sampled.

In order to obtain equilibrium properties from the trajectories sampled using metadynamics, a reweighting procedure is necessary that takes into account the time-dependent influence of the bias. In other words, a weight $w(\boldsymbol{s},t)$ has to be assigned to each sampled conformation of the system, which is dependent on the time evolution of the bias. Once we have that, we can measure equilibrium properties from the biased simulations:

$$\langle A\rangle_0 = \langle Aw\rangle_\mathrm{b}/\langle w\rangle_\mathrm{b} \quad (2)$$

where A is any observables defined on the system, the subscript 0 indicates the unbiased (i.e. equilibrium) average and the subscript b indicates the average done over the biased simulations.

Several reweighting techniques have been proposed for metadynamics simulation [33–37], which come with some limitations, for example, some of them are specifically suited for well-tempered metadynamics, which is a modified version of the original algorithm where the height of the Gaussians decreases during the simulation. The simulations we ran on Hazelhen to determine the conformational states of the fibrinogen complex [9] showed however that the popular reweighting scheme from Tiwary and Parrinello [37], when used to build the free energy landscape as a function of the collective variables, did not match exactly the negative bias potential, which also represents an estimate of the free energy of the system. Tiwary's method is based on the assumption that in between two Gaussian depositions, the system samples a biased energy function $U + V$ where U is the unbiased energy function of the system and V is the metadynamics bias. Thus the conformations of the system follow a canonical distribution with biased energy.

$$p_b(\boldsymbol{r},t) = \frac{\mathrm{e}^{-\beta(U(\boldsymbol{r})+V(\boldsymbol{s}(\boldsymbol{r}),t))}}{\int \mathrm{d}\boldsymbol{r}\mathrm{e}^{-\beta(U(\boldsymbol{r})+V(\boldsymbol{s}(\boldsymbol{r}),t))}} \quad (3)$$

For the unbiased system, however, we would have the following distribution:

$$p_0(\boldsymbol{r}) = \frac{\mathrm{e}^{-\beta U(\boldsymbol{r})}}{\int \mathrm{d}\boldsymbol{r}\mathrm{e}^{-\beta U(\boldsymbol{r})}} \quad (4)$$

We can then obtain the equilibrium distribution from the biased distribution by means of the following reweighting factor [34, 37]:

$$w(\boldsymbol{r},t) = \frac{p_0(\boldsymbol{r})}{p_b(\boldsymbol{r},t)} \tag{5}$$

$$= \mathrm{e}^{\beta V(\boldsymbol{s}(\boldsymbol{r}),t))} \frac{\int \mathrm{d}\boldsymbol{r} \mathrm{e}^{-\beta(U(\boldsymbol{r},t)+V(\boldsymbol{s}(\boldsymbol{r}),t))}}{\int \mathrm{d}\boldsymbol{r} \mathrm{e}^{-\beta U(\boldsymbol{r},t)}} \tag{6}$$

which can be further rewritten as [34, 37]:

$$w(\boldsymbol{r},t) = \mathrm{e}^{\beta V(\boldsymbol{s}(\boldsymbol{r}),t))} \frac{\int \mathrm{d}\boldsymbol{r} \int \mathrm{d}\boldsymbol{s}\ \delta(\boldsymbol{s}-\boldsymbol{s}(\boldsymbol{r}))\mathrm{e}^{-\beta(U(\boldsymbol{r},t)+V(\boldsymbol{s}(\boldsymbol{r}),t))}}{\int \mathrm{d}\boldsymbol{r} \int \mathrm{d}\boldsymbol{s}\ \delta(\boldsymbol{s}-\boldsymbol{s}(\boldsymbol{r}))\mathrm{e}^{-\beta U(\boldsymbol{r},t)}} \tag{7}$$

$$= \mathrm{e}^{\beta V(\boldsymbol{s}(\boldsymbol{r}),t))} \frac{\int \mathrm{d}\boldsymbol{s}\ p_0(\boldsymbol{s})\mathrm{e}^{-\beta V(\boldsymbol{s},t)}}{\int \mathrm{d}\boldsymbol{s}\ p_0(\boldsymbol{s})} \tag{8}$$

$$= \mathrm{e}^{\beta V(\boldsymbol{s}(\boldsymbol{r}),t))} \frac{\int \mathrm{d}\boldsymbol{s}\ \mathrm{e}^{-\beta F(\boldsymbol{s})}\mathrm{e}^{-\beta V(\boldsymbol{s},t)}}{\int \mathrm{d}\boldsymbol{s}\ \mathrm{e}^{-\beta F(\boldsymbol{s})}} \tag{9}$$

where

$$p_0(\boldsymbol{s}) = \int \mathrm{d}\boldsymbol{r}\delta(\boldsymbol{s}-\boldsymbol{s}(\boldsymbol{r}))p_0(\boldsymbol{r}) = \frac{\mathrm{e}^{-\beta F(\boldsymbol{s})}}{\int \mathrm{d}\boldsymbol{s}\ \mathrm{e}^{-\beta F(\boldsymbol{s})}} \tag{10}$$

is the unbiased distribution projected on the low-dimensional CV space Ω and $F(\boldsymbol{s})$ is the unbiased free energy.

Eq. 9, although formally exact, contains the term $F(\boldsymbol{s})$, which is not known a priori (it is actually often the main aim of the simulation). In metadynamics the negative bias potential asymptotically approximates the free energy of the system [14, 15, 36, 38]:

$$F(\boldsymbol{s}) \approx -\frac{\gamma}{\gamma-1}V(s,t) + c(t) \tag{11}$$

where γ is the so-called bias factor of well-tempered metadynamics, which goes to infinity in the case of standard metadynamics, and $c(t)$ is a time-dependent offset of the free energy profile. In the Tiwary and Parrinello method [37], $F(\boldsymbol{s})$ is approximated using eq. 11, leading to the following expression for the weight (for standard metadynamics):

$$w^{tw}(\boldsymbol{r},t) = \mathrm{e}^{\beta V(\boldsymbol{s}(\boldsymbol{r}),t)} \frac{\int \mathrm{d}\boldsymbol{s}}{\int \mathrm{d}\boldsymbol{s}\mathrm{e}^{\beta V(\boldsymbol{s},t)}} = \mathrm{e}^{\beta V(\boldsymbol{s}(\boldsymbol{r}),t)} \frac{1}{\langle \mathrm{e}^{\beta V(\boldsymbol{s},t)} \rangle_{\boldsymbol{s}}} \tag{12}$$

The approximation eq. 11, however, is only valid asymptotically, thus at short time scales the reweighting scheme may not provide accurate results.

Alternatively, we suggested [16] to approximate $F(\boldsymbol{s})$ with the value of the negative potential at the end of the simulation, which is supposedly more accurate:

$$w(\boldsymbol{r},t) = \mathrm{e}^{\beta V(\boldsymbol{s}(\boldsymbol{r}),t))} \frac{\int \mathrm{d}\boldsymbol{s}\ \mathrm{e}^{\beta(V(\boldsymbol{s},t_f)-V(\boldsymbol{s},t)}}{\int \mathrm{d}\boldsymbol{s}\ \mathrm{e}^{\beta V(\boldsymbol{s},t_f)}} \tag{13}$$

where t_f corresponds to the time at the end of the simulation. Eq. 13 would converge to eq. 12 at large t, but it will behave differently at small t. At short simulation times, a simple exponential reweighting would be more accurate than the Tiwary's eq. 12. A simple exponential reweighting, however, in the standard metadynamics setting where the bias increases with time would result in an underweighting of the initial part of the simulation. In ref. [16] we propose a simple way to correct it by subtracting the average value of the bias at every time step. This results in the balanced exponential reweighting:

$$w^{bex}(\boldsymbol{r},t) \propto e^{\beta V'(\boldsymbol{s}(\boldsymbol{r}),t)} = e^{\beta\left(V(\boldsymbol{s}(\boldsymbol{r}),t)-V_a(t)\right)} = e^{\beta V(\boldsymbol{s}(\boldsymbol{r}),t)}\frac{1}{e^{\beta\langle V(\boldsymbol{s},t)\rangle_{\boldsymbol{s}}}}. \tag{14}$$

The scheme proposed above differs from the previously proposed scheme of eq. 12 by the normalization factor of the exponential weight: in the case of eq. 12 the average value over Ω of the exponential of the bias potential is used, whereas in the new scheme eq. 14 we propose to use the exponential of the average bias. The average of the exponential (eq. 12) is very sensitive to small changes in the upper tail of the distribution of the bias potential and is, therefore, less robust in the initial part of the trajectory where the global free energy minimum of the system may not have been reached, yet.

The newly proposed scheme can be implemented without changes to the output of the popular metadynamics software PLUMED [39]. To demonstrate its advantages, we have tested it in several different scenarios and compared it with existing schemes. The standard mean of comparison that we have adopted consists in recovering the free energy landscape of a given system as a function of the collective variables by reweighting the conformations of the system sampled along the metadynamics trajectory. We did that for a series of systems for which an accurate free energy landscape is accessible and can be used as reference.

The first system we studied is a particle in a uni-dimensional double-well potential of the form $U(x) = (x^2 - 1)^2$. Simulations are performed at a temperature such that k_bT is 1/10 of the barrier separating the two energy wells. The system is discretized along the x direction into equally sized bins, and pseudo standard metadynamics simulation are performed by moving the particle to the left or right bin using a Metropolis criterion for accepting the move. The energy function for the Metropolis criterion is $U(x) + V(x,t)$, $V(x,t)$, where:

$$V(x,t) = \sum_{t'=\Delta t,2\Delta t,\ldots}^{t} \frac{v}{\sqrt{2\pi}\sigma} e^{\left(-(x-x(t'))^2/2\sigma\right)} \tag{15}$$

In the above expression, the metadynamics Gaussian hills have volume v (that is height $v/\sqrt{2\pi}\sigma$) and width σ. The deposition period is Δt. Several simulations were run using different metadynamics parameters but keeping the length and step size (bin width) fixed. We then estimated the free energy landscape of the system using eq. 12 and 14:

$$F_{est}(x,t) = -\beta^{-1} \log \left(\frac{\sum_{t'=0}^{t} \delta(x - x(t')) w(x(t'),t')}{\sum_{t'=0}^{t} w(x(t'),t')} \right) \tag{16}$$

where the δ functions are the characteristic functions of the discrete bins along the x axis.

In Fig. 3a we report the estimated and reference free energy landscape of the system as a function of the simulated time. We repeated the simulations 72 times with different initial conditions and measured the error of the estimated free energy with respect to the reference in each of the simulations (the error is computed as the root-mean-square deviation of the two free energy profiles limited to the interval (-2,2) after subtracting the average). The data (Fig. 3b) show that the estimate obtained with the newly proposed eq. 14 converges faster than the other tested methods to the reference landscape. Also other estimates of the quality of the free energy landscape, like the estimate of the free energy difference between the minima (Fig. 3c) and the estimate of the height of the barrier (Fig. 3d) reveal a similar picture. Another advantage of the balanced exponential reweighting is the low run-to-run variability reported by the error bar in Fig.3b-d. A detailed look at the weights of the sampled conformations (Fig. 3) shows that while the balanced exponential weights are generally constant along the simulation, they are smaller than average in the very initial part of the simulation when the system has not yet explored both minima. On the other hand, Tiwary's method produces weights that are larger than average in the initial part of the simulation. This overestimate reduces the quality of the free energy profile for the early part of the run.

Although the uni-dimensional system offers already a good overview of the advantages of the newly proposed reweighting scheme, a test with a more realistic system is necessary to assess the performance in a normal-use scenario. For that, in the same work [16], we used an alanine dipeptide, which represents a standard benchmark of enhanced sampling techniques. The alanine dipeptide can be considered as the smallest protein-like unit as its structure can be characterized by the two protein backbone dihedral angles ϕ and ψ. We performed the metadynamics simulations using GROMACS [17] with the PLUMED [39] plugin. The system was simulated for short trajectories (8 ns) in vacuum using the standard force field AMBER03 [40] and standard values for time step and non-bonded interaction cutoff. The backbone dihedral angles ϕ and ψ were biased during the metadynamics simulations (for all the details of the simulations and the set of metadynamics parameters used please refer to our original work [16]). Adopting a strategy similar to the uni-dimensional case, we estimated the free energy landscape of the system as a function of ϕ and ψ using several different reweighting schemes including the newly proposed balanced exponential. We did that at several different time points along the simulation. We then compared the free energy estimates with the reference obtained by running an extremely long well-tempered metadynamics simulations (Fig. 4).

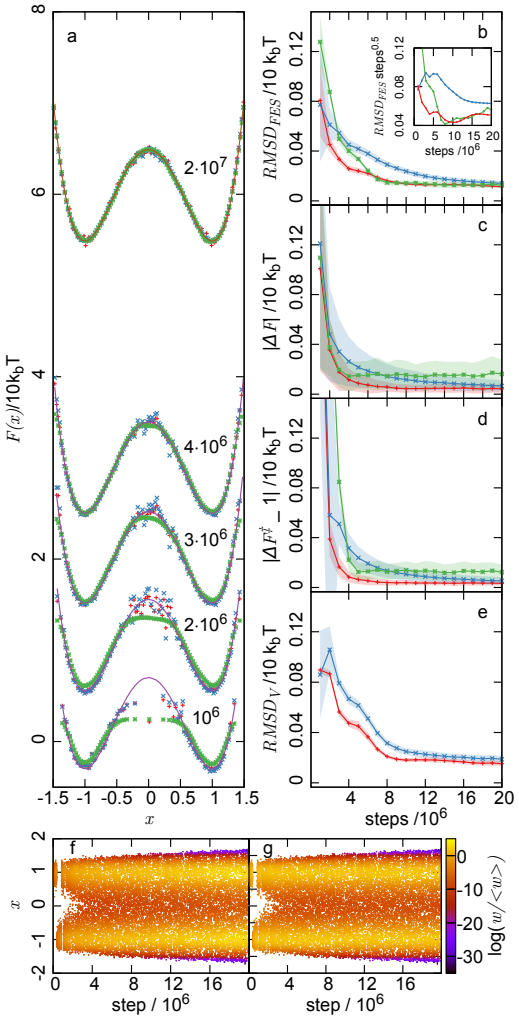

Fig. 3: (a) FES obtained along a single run at different trajectory lengths using balanced exponential reweighting, Tiwary reweighting and negative bias potential (red, blue and green points, respectively). The reference FES is plotted in purple. (b-e) Time series of (b) the RMSD (in inset is the RMSD$\cdot\sqrt{(t)}$), (c) estimated free energy difference between the two minima (absolute value), (d) estimated error on height of free energy barrier, and (e) the RMSD between reweighted FES and negative bias. Same color scheme as in part a. The solid lines represent the average values of the quantities across the 72 independent runs. Shaded bands indicate the standard deviations. (f-g) Time series of the position of the particle along one run where balanced exponential (f) and Tiwary (g) weights are reported according to a color scale. Adapted with permission from ref. [16], ©2020 American Chemical Society.

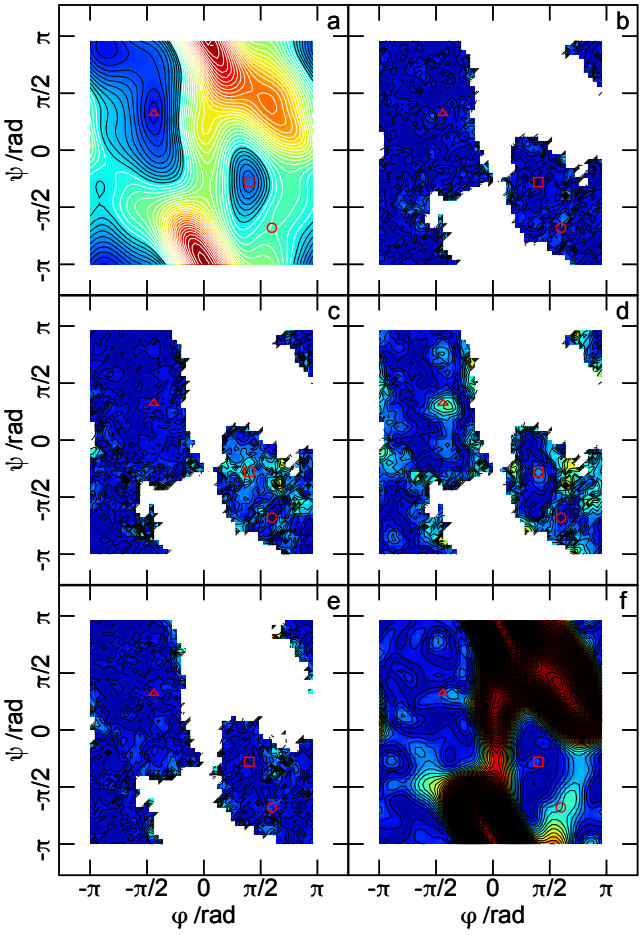

Fig. 4: (a) Reference FES of the alanine dipeptide as a function of the CV ϕ and ψ. Contour levels are plotted every 1 kbT. The black contours indicate the region within 10 kbT from the global minimum, which is used for the RMSD calculations. The red triangle, square and circle indicate the position of the minima $C7_{eq}$ and C_{ax} and the transition state ‡, respectively. The color shades are guides for the eye. (b-f) Difference between the reference FES and those estimated using the balanced exponential, Tiwary's, Branduardi's, and Bonomi's reweighting, and the negative bias, respectively, after 1.4 ns in one of the runs. Contour levels are plotted every 0.25 kbT, and the range of color shades is 4 times smaller than that in part a. Adapted with permission from ref. [16], ©2020 American Chemical Society.

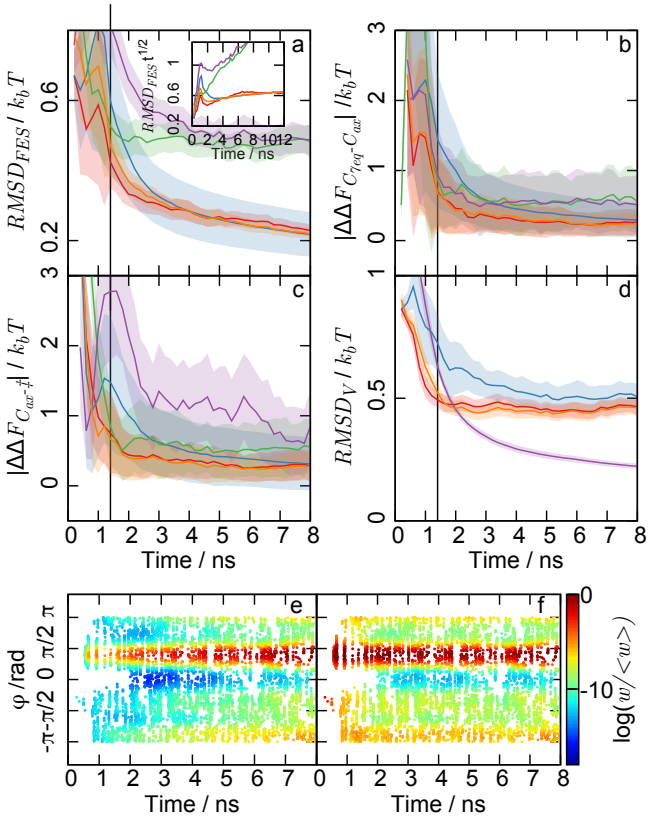

Fig. 5: (a), (b) and (c) provide the time series of the $RMSD$ from reference FES, and the error on the $\Delta F_{C_{7eq}-C_{ax}}$ and $\Delta F_{C_{ax}-\ddagger}$, respectively, for the balanced exponential (red), Tiwary's (blue), Branduardi's (purple), Bonomi's (orange) reweighting and negative bias (green) estimate of the FES. The data are averaged over 96 runs. Shaded bands indicate standard deviations. The black line at 1.4 ns indicates the time point where the FES in Fig. 4 have been extracted. (a inset) the $RMSD_{FES}\sqrt{t}$ shows to approximately reach a plateau for balanced exponential, Tiwary's and Bonomi's reweighting schemes. (d) $RMSD_V$ between the different reweighting schemes and negative bias (same color scheme as above). (e), (f) Time series of ψ when ϕ=-1.88 rad along one selected run. Balanced exponential (e) and Tiwary (f) weights are reported according to the color scale. $\langle w \rangle$ is the average of the weights along the run. Adapted with permission from ref. [16], ©2020 American Chemical Society.

The results obtained in this test confirmed the observations made in the unidimensional case (Fig. 5): the balanced exponential reweighting scheme converges faster than most of the other methods to the reference free energy landscape, with the exception of the method by Bonomi et.al [34], which, as we demonstrate in ref. [16], within some limits, may provide similar but not better results.

We also tested the newly developed algorithm in other scenarios: the reweighting of observables not biased in the metadynamics simulation and in well-tempered metadynamics. In all tested scenarios the balanced exponential reweighting provided similar or faster convergence than the other methods and, in addition, lower run-to-run fluctuations. We refer the interested reader to our original publication [16] for further details.

4 Conclusions

In this report, we have summarized the results obtained for our projects using the computational resources made available by the HLRS Stuttgart with the Hazelhen and Hawk HPC infrastructure. We show how molecular dynamics simulations of the tumor suppressor protein p53, an important target in cancer research, have been used to understand the effect of cancer mutations on the stability of the protein as well as the stabilizing effect of ligands binding to a mutation-induced pocket on the protein surface. In addition, we proposed an improved reweighting method for the analysis of metadynamics simulations, which is particularly useful in the context of large MD simulations of complex systems where, due to the high computational cost, fast convergence to the underlying free energy landscape is essential.

Acknowledgements This work was partly funded by the German Research Foundation (DFG) grant SFB1066 project Q1 and SFB TRR 146 as well as DFG grant JO 1473/1-1 and Worldwide Cancer Research (grants 14-1002, 18-0043). We gratefully acknowledge support with computing time from the HPC facility Hazelhen and Hawk at the High Performance Computing Center Stuttgart (HLRS) project Flexadfg and the HPC facility Mogon at the University of Mainz.

References

1. K. Lindorff-Larsen, S. Piana, R.O. Dror, D.E. Shaw, Science **334**(6055), 517 (2011)
2. N. Basse, J. Kaar, G. Settanni, A. Joerger, T. Rutherford, A. Fersht, Chemistry and Biology **17**(1) (2010)
3. S. Köhler, F. Schmid, G. Settanni, PLoS Computational Biology **11**(9) (2015)
4. S. Köhler, F. Schmid, G. Settanni, Langmuir **31**(48), 13180 (2015)
5. G. Settanni, J. Zhou, T. Suo, S. Schöttler, K. Landfester, F. Schmid, V. Mailänder, Nanoscale **9**(6) (2017)
6. G. Settanni, J. Zhou, F. Schmid, Journal of Physics: Conference Series **921**(1), 012002 (2017)
7. G. Settanni, T. Schäfer, C. Muhl, M. Barz, F. Schmid, Computational and Structural Biotechnology Journal **16**, 543 (2018)

8. S. Köhler, F. Schmid, G. Settanni, in *High Performance Computing in Science and Engineering '16: Transactions of the High Performance Computing Center Stuttgart (HLRS) 2016* (Springer International Publishing, 2017), pp. 61–78
9. T. Schäfer, J. Zhou, F. Schmid, G. Settanni, *Blood proteins and their interactions with nanoparticles investigated using molecular dynamics simulations* (2018)
10. T. Schafer, C. Muhl, M. Barz, F. Schmid, G. Settanni, in *High Performance Computing in Science and Engineering ' 18* (Springer International Publishing, 2019), pp. 63–74
11. T. Schäfer, C. Muhl, M. Barz, F. Schmid, G. Settanni, in *High Performance Computing in Science and Engineering '19* (Springer International Publishing, Cham, 2021), pp. 65–76
12. A.C. Joerger, A.R. Fersht, Annual Review of Biochemistry **85**, 375 (2016)
13. A. Laio, M. Parrinello, Proceedings of the National Academy of Sciences of the United States of America **99**(20), 12562 (2002)
14. G. Bussi, A. Laio, M. Parrinello, Physical review letters **96**(9), 090601 (2006)
15. A. Barducci, G. Bussi, M. Parrinello, Physical Review Letters (2008)
16. T.M. Schäfer, G. Settanni, Journal of Chemical Theory and Computation **16**(4), 2042 (2020)
17. H.J.C. Berendsen, D. van der Spoel, R. van Drunen, Computer Physics Communications **91**(1–3), 43 (1995)
18. J. Huang, S. Rauscher, G. Nawrocki, T. Ran, M. Feig, B.L. De Groot, H. Grubmüller, A.D. MacKerell, Nature Methods **14**(1), 71 (2016)
19. K. Vanommeslaeghe, E. Hatcher, C. Acharya, S. Kundu, S. Zhong, J. Shim, E. Darian, O. Guvench, P. Lopes, I. Vorobyov, A.D. Mackerell, J. Comput. Chem. **31**(4), 671 (2010)
20. B. Hess, H. Bekker, H.J.C. Berendsen, J.G.E.M. Fraaije, LINCS: A Linear Constraint Solver for Molecular Simulations. Tech. rep. (1997)
21. M.P. Allen, D.J. Tildesley, *Computer Simulation of Liquids* (Clarendon Press., 1987)
22. U. Essmann, L. Perera, M.L. Berkowitz, T. Darden, H. Lee, L.G. Pedersen, The Journal of Chemical Physics **103**(19), 8577 (1995)
23. W.L. Jorgensen, J. Chandrasekhar, J.D. Madura, R.W. Impey, M.L. Klein, Journal of Chemical Physics **79**(2), 926 (1983)
24. M. Parrinello, A. Rahman, Physical Review Letters **45**(14), 1196 (1980)
25. S. Nosé, The Journal of Chemical Physics **81**(1), 511 (1984)
26. W.G. Hoover, Physical Review A **31**(3), 1695 (1985)
27. A.C. Joerger, M.D. Allen, A.R. Fersht, Journal of Biological Chemistry **279**(2), 1291 (2004)
28. M.R. Bauer, A. Krämer, G. Settanni, R.N. Jones, X. Ni, R. Khan Tareque, A.R. Fersht, J. Spencer, A.C. Joerger, ACS Chemical Biology **15**(3), 657 (2020)
29. W. Humphrey, A. Dalke, K. Schulten, Journal of Molecular Graphics **14**, 33 (1996)
30. M. Seeber, M. Cecchini, F. Rao, G. Settanni, A. Caflisch, Bioinformatics **23**(19), 2625 (2007)
31. M.R. Bauer, R.N. Jones, R.K. Tareque, B. Springett, F.A. Dingler, L. Verduci, K.J. Patel, A.R. Fersht, A.C. Joerger, A.C. Joerger, Future Medicinal Chemistry **11**(19), 2491 (2019)
32. G. Interlandi, S.K. Wetzel, G. Settanni, A. Plückthun, A. Caflisch, Journal of Molecular Biology **375**(3), 837 (2008)
33. G. Tiana, European Physical Journal B **63**(2), 235 (2008)
34. M. Bonomi, A. Barducci, M. Parrinello, Journal of Computational Chemistry **30**(11), 1615 (2009)
35. J. Smiatek, A. Heuer, Journal of Computational Chemistry **32**(10), 2084 (2011)
36. D. Branduardi, G. Bussi, M. Parrinello, Journal of Chemical Theory and Computation (2012)
37. P. Tiwary, M. Parrinello, The Journal of Physical Chemistry B **119**(3), 736 (2015)
38. J.F. Dama, M. Parrinello, G.A. Voth, Physical Review Letters **112**(24), 240602 (2014)
39. G.A. Tribello, M. Bonomi, D. Branduardi, C. Camilloni, G. Bussi, Computer Physics Communications **185**(2), 604 (2014)
40. D.A. Case, T.E. Cheatham, T. Darden, H. Gohlke, R. Luo, K.M. Merz, A. Onufriev, C. Simmerling, B. Wang, R.J. Woods, Journal of Computational Chemistry **26**(16), 1668 (2005)

Hadronic contributions to the anomalous magnetic moment of the muon from Lattice QCD

M. Cè, E.-H. Chao, A. Gérardin, J.R. Green, G. von Hippel, B. Hörz, R.J. Hudspith, H.B. Meyer, K. Miura, D. Mohler, K. Ottnad, S. Paul, A. Risch, T. San José and H. Wittig

Abstract The recently reported new measurement of the anomalous magnetic moment of the muon, a_μ, by the E989 collaboration at Fermilab has increased the tension with the Standard Model (SM) prediction to 4.2 standard deviations. In order to increase the sensitivity of SM tests, the precision of the theoretical prediction, which is limited by the strong interaction, must be further improved. In our project we employ lattice QCD to compute the leading hadronic contributions to a_μ and various other precision observables, such as the energy dependence ("running") of the electromagnetic coupling, α, and the electroweak mixing angle, $\sin^2\theta_W$. Here we report on the performance of our simulation codes used for the generation of gauge ensembles at (near-)physical pion masses and fine lattice spacings. Furthermore, we present results for the hadronic running of α, the electroweak mixing angle, as well

H.B. Meyer, K. Miura, T. San José and H. Wittig
Helmholtz Institut Mainz, Johannes Gutenberg Universität, 55099 Mainz, Germany

K. Miura, D. Mohler and T. San José
GSI Helmholtzzentrum für Schwerionenforschung, Darmstadt, Germany

M. Cè and J. R. Green
Theoretical Physics Department, CERN, Geneva, Switzerland

E.-H. Chao, G. von Hippel, R.J. Hudspith, H.B. Meyer, K. Ottnad, S. Paul, T. San José and H. Wittig
Institut für Kernphysik and PRISMA$^+$ Cluster of Excellence, Universität Mainz, Johann-Joachim-Becher-Weg 45, D-55099 Mainz, Germany

A. Risch
John von Neumann Institute for Computing NIC, Deutsches Elektronen-Synchrotron DESY, Platanenallee 6, 15738 Zeuthen, Germany

A. Gérardin
Aix Marseille Univ, Université de Toulon, CNRS, CPT, Marseille, France

B. Hörz
Nuclear Science Division, Lawrence Berkeley National Laboratory, Berkeley, CA 94720, USA

K. Miura
Kobayashi-Maskawa Institute for the Origin of Particles and the Universe, Nagoya University, Nagoya 464-8602, Japan

W. E. Nagel et al. (eds.), *High Performance Computing in Science and Engineering '21*,
https://doi.org/10.1007/978-3-031-17937-2_2

as the hadronic vacuum polarisation and light-by-light scattering contributions to a_μ. Results from an ancillary calculation of the spectrum in the isovector channel are crucial in order to further increase the precision of our determination of the hadronic vacuum polarisation contribution.

1 Introduction

The Standard Model of Particle Physics provides a quantitative and precise description of the properties of the known constituents of matter in terms of a uniform theoretical formalism. However, despite its enormous success, the Standard Model (SM) does not explain some of the most pressing problems in particle physics, such as the nature of dark matter or the asymmetry between matter and antimatter. The world-wide quest for discovering physics beyond the SM involves several different strategies, namely (1) the search for new particles and interactions that are not described by the SM, (2) the search for the enhancement of rare processes by new interactions, and (3) the comparison of precision measurements with theoretical, SM-based predictions of the same quantity. These complementary activities form an integral part of the future European strategy for particle physics [1].

Precision observables, such as the anomalous magnetic moment of the muon, a_μ, have provided intriguing hints for the possible existence of "new physics". The longstanding tension between the direct measurement of a_μ and its theoretical prediction has recently increased to 4.2 standard deviations, following the publication of the first result from the E989 experiment at Fermilab [2]. As E989 prepares to improve the experimental precision further, it is clear that the theoretical prediction must be pushed to a higher level of accuracy as well, in order to increase the sensitivity of the SM test. Since the main uncertainties of the SM prediction arise from strong interaction effects, current efforts are focussed on quantifying the contributions from hadronic vacuum polarisation (HVP) and hadronic light-by-light scattering (HLbL). This has also been emphasised in the 2020 White Paper [3] in which the status of the theoretical prediction is reviewed.

Our project is focussed on calculations of the hadronic contributions to the muon anomalous magnetic moment from first principles, using the methodology of Lattice QCD. To this end, we perform calculations of the HVP contribution at the physical value of the pion mass, in order to reduce systematic errors. Another highly important ingredient of our calculation is the determination of the spectrum in the isovector channel of the electromagnetic current correlator, which constrains the long-distance contribution to the HVP. Our group has also developed a new formalism for the direct calculation of the HLbL contribution, which has produced the most precise estimate from first principles so far [4].

The HVP contribution to the muon anomalous magnetic moment is closely linked to the hadronic effects that modify the value of the electromagnetic coupling, $\Delta\alpha$. Since $\Delta\alpha$ depends on other SM parameters such as the mass of the W-boson, a precise determination provides important information for precision tests of the SM. Finally,

we also compute the hadronic contributions to the "running" of the electroweak mixing angle, a precision observable which is particularly sensitive to the effects of physics beyond the SM in the regime of low energies.

2 Computational setup

One of the major computational tasks of our project is the generation of gauge-field ensembles at (close to) physical light-quark masses. For a particular challenge encountered in these simulations please refer to [5]. The generation of a gauge field ensemble dubbed E250 at physical pion and kaon masses has been a long standing goal of our programme on Hazel Hen and Hawk, and has been finalized since the last report. Furthermore we recently produced two somewhat coarser lattices named D452 and D152[1] at light pion masses. For both ensembles, the generation of 500 gauge field configurations, corresponding to 2000 molecular dynamics units (MDU) had been proposed. As it turned out, the rather coarse lattice spacing of D152 lead to sustained algorithmic problems, hence the run was stopped after 275 gauge configurations (1100 MDU). For D452 no such issues were observed, and we were able to produce 1000 gauge configurations (4000 MDU) due to better than expected performance for this run. Preliminary results for observables suggest that ensemble D452 will play a vital role for obtaining more precise results for the observables in our project.

Figure 1 shows the Hamiltonian deficits ΔH as well as the Monte Carlo history of the topological charge for ensembles E250 and D452. The acceptance rate resulting from the history of ΔH is $(87.1 \pm 1.0)\%$ for E250 and $(91.5 \pm 0.7)\%$ for D452. The generation of these chains is now complete and the calculation of physics observables has been started on compute clusters operated by JGU Mainz.

The `openQCD` code used in our calculations exhibits excellent scaling properties over a wide range of problem sizes. Figure 3 shows the strong-scaling behaviour for the system size corresponding to ensemble D452, i.e. for a 128×64^3 lattice, as measured on Hawk (left pane). The timings refer to the application of the even-odd preconditioned O(a) improved Wilson–Dirac operator $\hat{D}_{\mathrm{w}}$ to a spinor field which accounts for the largest fraction of the total computing time for several of our projects.

For the gauge field generation runs on Hawk and for the HLbL runs on lattices of size 128×64^3 we used the following setup:

A Local lattice volume of size 8^4 per MPI rank with 8192 MPI ranks on 64 nodes.

In addition to this setup, we performed spectroscopy runs on J303 (192×64^3) with setup B and on E250 192×96^3 with setup C:

B Local lattice of size 12×8^3 per MPI rank with 8192 MPI ranks on 64 nodes.
C Local lattice volume of size $12 \times 6^2 \times 12$ per MPI rank with 32768 MPI ranks on 256 nodes.

[1] This ensemble was called D151 in the proposal.

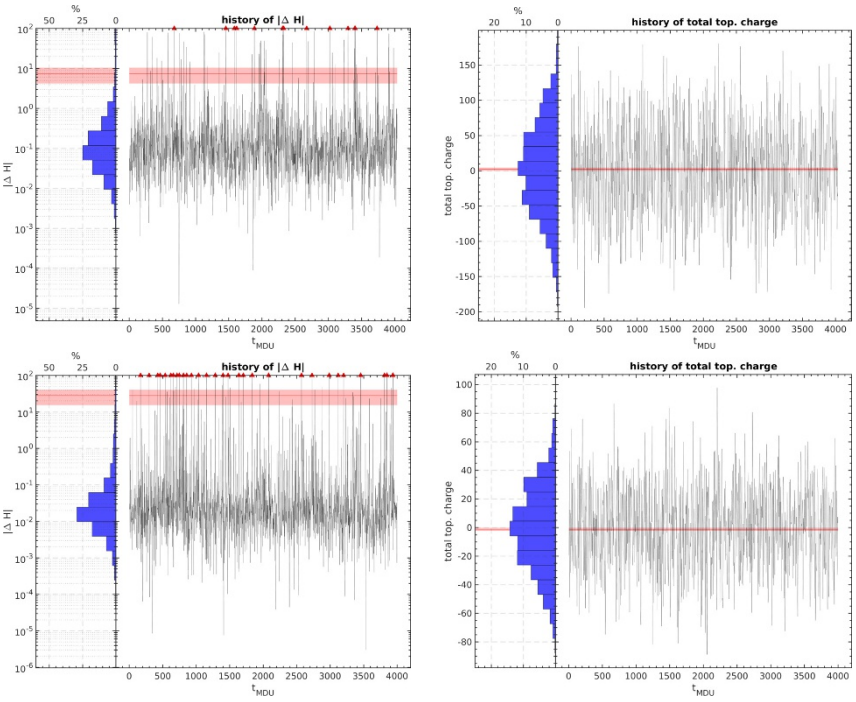

Fig. 1: Monte-Carlo histories of the Hamiltonian deficit ΔH (left) and the total topological charge (right) for E250 (top) and D452 (bottom).

When possible a hypercube of size $2^2 \times 4^2$ processes was grouped onto a single CPU, to minimise off-CPU communication.

For the current allocation year we received a total of 100 MCore hours. It was foreseen that 32% / 40% / 27% would be spent on the gauge field generation / HVP spectroscopy / HLbL respectively, while the actual percentages of computing time spent by the time of writing this report are given by 30% / 44% / 26%.

3 The hadronic running of the electroweak couplings

We start our discussion of precision observables with the hadronic contributions to the energy dependence ("running") of the electromagnetic coupling, α, since its calculation shares many features and definitions with the determination of the HVP contribution to the muon anomalous moment.

The electromagnetic coupling in the Thomson limit is one of the most precisely known quantities, $\alpha = 1/137.035999084(21)$ [6]. However, for scales above a few hundred MeV, the low-energy hadronic contribution to the vacuum polarization

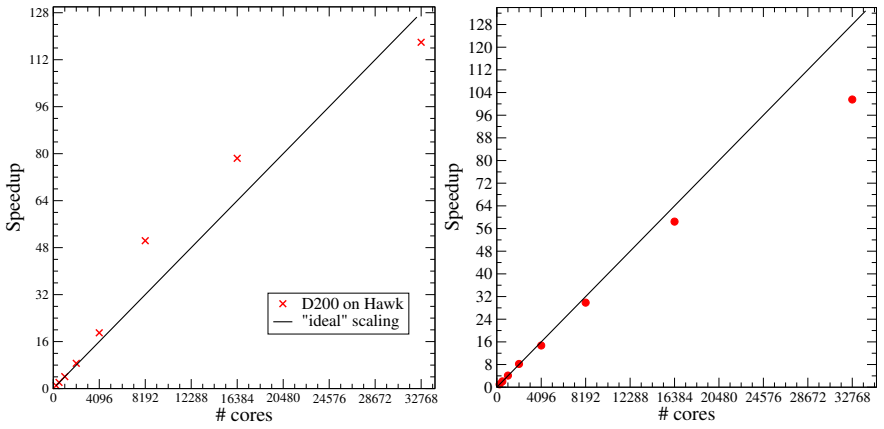

Fig. 2: Left: Strong-scaling behaviour of the `openQCD` code on Hawk. The plot shows the application of the even-odd preconditioned Wilson–Dirac operator on a 128×64^3 lattice. Speedup factors are defined relative to 256 cores. A clear indication of hyperscaling is seen in this regime. Right: Weak scaling with a local volume of 8^4 on Hawk.

induces a theoretical uncertainty. If one parameterizes the energy dependence, or "running", of the coupling in the so-called on-shell scheme,

$$\alpha(q^2) = \frac{\alpha}{1 - \Delta\alpha(q^2)}, \tag{1}$$

the five flavour quark contribution at the Z-pole is found to be $\Delta\alpha^{(5)}_{\rm had}(M_Z^2) = 0.02766(7)$ [6]. Its poorer precision is a limiting factor for the global fit of the electroweak sector of the Standard Model (SM). Thus, the goal is to improve the precision of this estimate, by reducing the uncertainties associated with the strong interaction. We concentrate on the quark contribution at low energies, which is given by the one-subtracted dispersion relation

$$\Delta\alpha_{\rm had}(q^2) = 4\pi\alpha\bar{\Pi}^{\gamma\gamma}(q^2), \qquad \bar{\Pi}^{\gamma\gamma}(q^2) = {\rm Re}\left[\Pi^{\gamma\gamma}(q^2) - \Pi^{\gamma\gamma}(0)\right]. \tag{2}$$

The standard method to obtain eq. (2) employs the optical theorem, which relates the HVP function with the so-called R-ratio, i.e. the total hadronic cross section $\sigma(e^+e^- \to \text{hadrons})$ normalized by $\sigma(e^+e^- \to \mu^+\mu^-)$, via a dispersion integral. While the integral can be evaluated using experimental data for the R-ratio in the low-energy domain, this procedure introduces experimental uncertainties into a theoretical prediction. Therefore, lattice computations in the space-like region $Q^2 = -q^2$ provide a valuable *ab initio* crosscheck. In order to estimate $\Delta\alpha^{(5)}_{\rm had}(M_Z^2)$, we use the so-called Euclidean split technique [7, 8]